CHAPTER II

LITERATURE REVIEW

2.1 Structure of Solid Hydrates

2.1.1 Coordination and Bonding of Water Molecules

Chidabaram et al.[15] had classified three types of coordination of water molecules as shown in Figure 2.1 , namely, trigonal, pyramidal and tetrahedral surrounding. This classification can be subdivided into 11 categories as shown in Table 2.1. Although various classifications are reported in the literatures [16-19] in order to describe the environment of H_2O molecules in solid hydrates, Chidabaram et al. classification is most commonly reported.
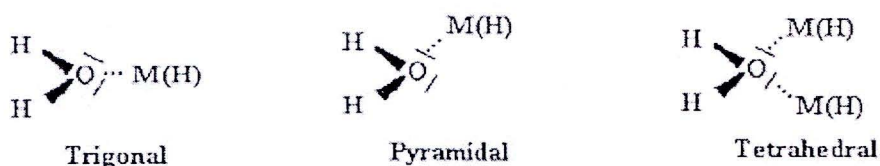

Figure 2.1   Coordination of water molecules in solid hydrates.

Table 2.1   Classification of water molecules in solid hydrates with respect to their lone pair coordination

Type	Lone-pair coordination	Polyhedron	Class
A	Lone-pair toward two M^+	Tetrahedral	2
B	Lone-pair toward two M^{n+}	Tetrahedral	2
C	Bisectrix toward M^+	Trigonal	1
D	Bisectrix toward M^{n+}	Trigonal	1
E	Lone-pair toward two H	Tetrahedral	2
F	Bisectrix toward H	Trigonal	1
G	Lone-pair toward two M^+ and H	Tetrahedral	2
H	Lone-pair toward two M^{n+} and H	Tetrahedral	2
I	One lone-pair toward two M^+	Pyramidal	1'
J	One lone-pair toward two M^{n+}	Pyramidal	1'
K	One lone-pair toward two H	Pyramidal	1'

The hydrogen bonds can be linear, bent, or bifurcated. However, H-bonds tend to be linear and the proton acceptors tend to be located close to the water plane. Especially with increasing bond strengths, deviations from linearity decrease, i.e., OH···Y angle ≈ 180°. Furthermore, hydrogen bonds are called to be symmetric and asymmetric (Figure 2.2). The structural arrangement of the hydrogen-bond donor and accepter groups strongly influence the strength of hydrogen bonds. The hydrogen bonding effects the geometric structure of OH···Y grouping and the coordination as well as the configuration of the hydrogen-bond donor and accepter atom H and Y. Most frequent types are more or less linear hydrogen bonds with OH···Y hydrogen-bond angles ≈ 180° , bent hydrogen bonds with hydrogen-bond angles << 180°, and bifurcated hydrogen-bond (Figure 2.2) [x].
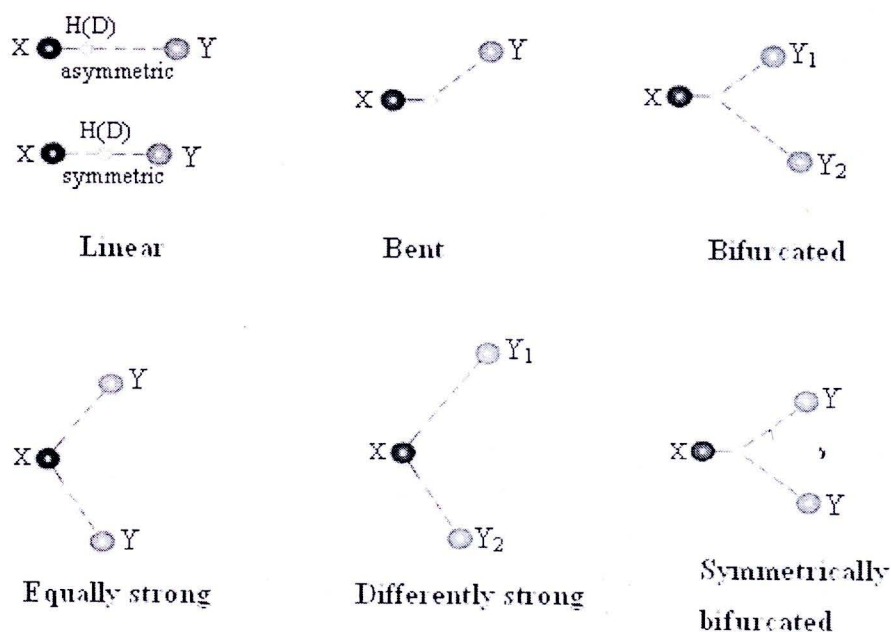

Figure 2.2 Various structures of hydrogen bonds [49].

2.2 Hydrogen Bonding Interaction

The hydrogen bond is the term giving to the relatively weak secondary interaction between an H atom bound to an electronegative atom and another electronegative atom, which has one or more lone pairs and can thus act as a base.

The proton donors, X-H, and proton acceptors, Y, interact with each other through a hydrogen bond and generally represented as:

$$\overset{\delta^{-}}{\text{X}}\text{—}\overset{\delta^{+}}{\text{H}}\cdots\text{Y}$$
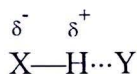
Such interaction is strongest when both X and Y are highly electronegative elements. The main donors are N-H, O-H and F-H, and the most commonly encountered hydrogen bonds are O—H$\cdots$O and N—H$\cdots$O.

Many of the earlier experimental evidences for hydrogen bonding came from the comparisons of the physical properties of hydrogen compounds such as boiling point and heat of vaporization. Hydrogen bonding has been extensive studied by means of infrared and Raman spectroscopies. When the X-H group encounters the hydrogen bonding, there are three main changes in vibrational spectra (IR, Raman) [20]

(1) The X-H bending frequency is usually increased.

(2) The X-H stretching frequency is lowered relative to that in the free molecule.

(3) The band due to the X-H strectching is substantially broadened and the intensity also increased marked.

The geometry of an isolated water molecule in the gas phase is a well known from spectroscopic measurements and illustrated in Figure 2.3.
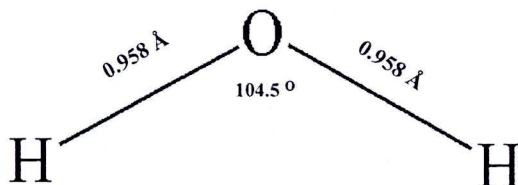

Figure 2.3 The geometry of an isolated water molecule [28].

Potential energy curves [21] of the interaction between two water molecules with different orientations are explained in Figure 2.4. Orientation A shows strong

repulsion when two lone-pair electrons of two water molecules point directly to each other [19]. The B and C curves demonstrate different attraction orientations [22].
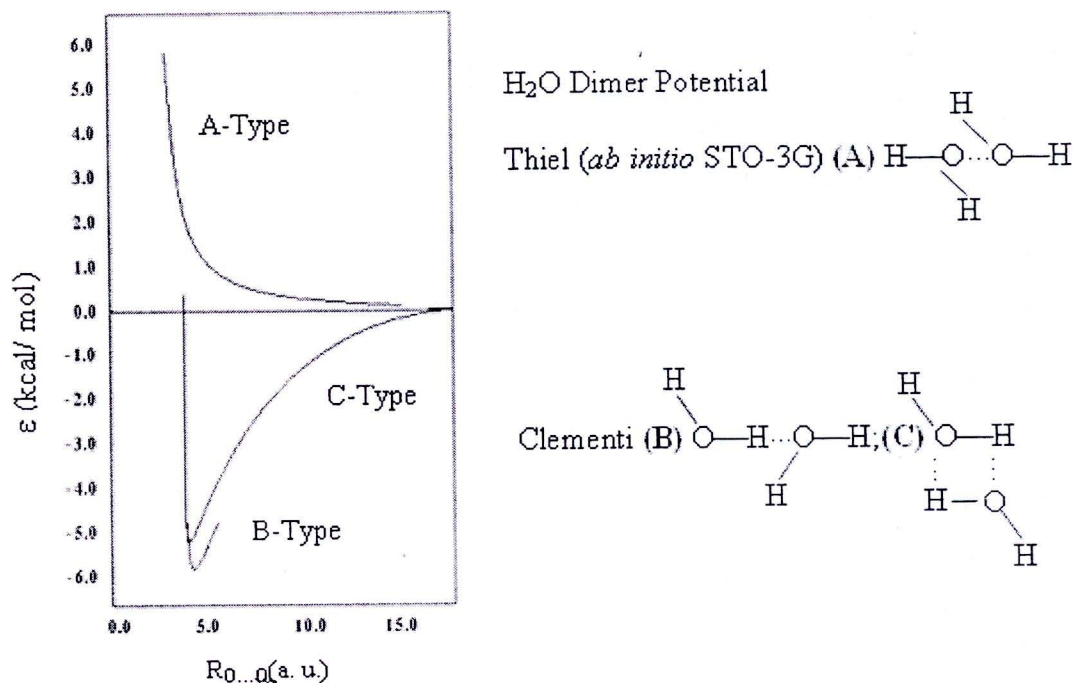

Figure 2.4 Potential energy curves of water dimer with different orientations calculated by quantum chemical method, A: repulsion potential [19], B: linear dimer (Clementi), C: cyclic dimer (Clementi) [19-23].

2.3 Angle Dependence of Hydrogen Bond

Luck and coworkers [24-26] had studied intensively about the angle dependence of H-bonding. It was claimed that there is lacking of the experimental data on the angle dependence of H-bond energy. Theoretically, one would expect the orientational dependence of H-bond energy [27]. In hydrates, angle β values (see Figure 2.5a) were found to be mostly about 5-15°. The values of $\beta > 40°$ of some hydrates were reported as well. In such highly bent H-bond, the H-bond interaction energy is expected to be very weak so that another proton acceptor is needed [28-30]. The branching of H-bonds on donor proton will be latter on referred to as "bifurcated", if two acceptors. Theoretically, β_1 and β_2 shown in Figure 2.5b, in bifurcated hydrogen bonding should be equal. Some crystal hydrates showed $\beta_1 \neq \beta_2$

[28]. Survey values of ΔH_β / $\Delta H_{\beta=0}$ as a function of angle β were reported by Luck [27]. In relation to the angle dependence of H-bond enthalpy, Brown [30] and Hamilton [31] have shown that in crystal hydrates there is a correlation between the X...Y distance and the X-H...Y angle, in such a way that, the angle increase from $\beta = 0$ (strong H-bonds) to around $\beta = 50°$ for the weak one. Secondary effect of high β angle could be related with the low bond valence of the acceptor H...Y bond which induces the formation of bifurcated H-bond. The tendency of H-bond to form angle $\beta = 0$ undoubtly has great significance for biochemistry. This is an indication of the specificity of biochemical structures, for instance, pair of bases in DNA are connected by H-bonds via six-membered rings with $\beta = 0$ [27]. In addition, in the α-helix of protein the individual helix coils are bonded to one another by H-bonds with $\beta = 0$.
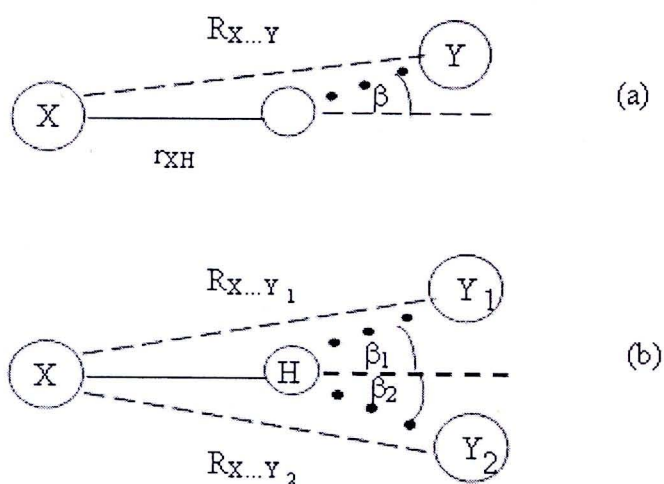

Figure 2.5   (a) H-bond interaction between a donor system X-H and the lone pair of electron of an acceptor Y depends on the bond angle β between X-H axes of lone-pair of electron orbital [27]. X-H bond is "donor bond" and H...Y is acceptor bond [30]. and (b) "Bifurcated H-bond" on H of X-H group with two proton acceptor Y_1, and Y_2, $R_{X...Y1}$ and $R_{X...Y2}$ are the distances from atom X to Y_1 and Y_2, and the H-bond angle are β_1 and β_2, respectively.

2.4 Distance Dependence of O – H. . .Y Hydrogen Bond

The discussion about hydrogen bonds based on spectroscopic and crystallographic data reported in the literatures leads to the following information. Rundle and Parasol [32] found an asymptotic dependence of v_{OH} on O. . .O distance, whereas in a smaller distance range Lord and Merrifield [33] found a linear relation between Δv and $R_{O...O}$. Similarly Pimentel and Sederholm [34] found the linear relationships but with different slopes for O – H ...O, N – H ...O, and N – H ...N hydrogen bonds. They expressed the equation for O – H ...O type in the following form:

$$\Delta v(O – H ...O) = 4.43 \times 10^{3} (cm^{-1}/Å) \ (2.84 – R) \ (Å) \qquad ...(1)$$

Where Δv is in cm^{-1} and R is the distance (Å). In crystalline hydrates similar correlations were found experimentally by Glemser and Hartert [35] and other investigators. In 1973, Falk and Knop [36] expressed the distance dependence of v_{OD} (HOD) in hydrates as follow:

$$R = c \ ln(d \ / \ \Delta v_{OD}(cm^{-1})) \qquad ...(2)$$

Where c = 0.1391 Å, ln d = 25.56 and Δv_{OD} is in cm^{-1}. Subsequently, Falk [37] expressed the relation between R and Δv_{OD}(HOD), as reported by Scherer [38] in the form:

$$v_{OD}(HOD) = v_{OD}(HOD)_{vap} – exp \ (k – 1..R_{O...O}) \qquad ...(3)$$

where $v_{OD}(HOD)_{vap}$ = 2727 cm^{-1} , k = 20.96, 1. = 5.539 (Å)$^{-1}$. The eq.(3) in form of eq.(2) provides c = 0.1805 Å , and ln d = 20.96. Eq. (3) can be rearranged to eq. (2), but gives some different constant values. Asymptotic limit is the gas phase value (2727 cm^{-1} for v_{OD}). Novak [39] published the correlation curve between v_{OH}(HOD) and $R_{O...O}$ in the region of 2.43 to 2.90 Å, but as reviewed by Scherer, no correlation equation was given. During 1978 - 1981, Berglund and coworkers [40] reported the

correlation between $\nu_{OD}(HOD)$ and $R_{O...O}$ in some hydrates. Their correlation equation is

$$\nu_{OD}(HOD) = \nu_{OD}(HOD)_{vap} - m. \exp(-n. R_{O...O}) \qquad ...(4)$$

where $\nu_{OD}(HOD)_{vap} = 2727$ cm^{-1}, m = 8.97 x 10^6 cm^{-1}, n = 3.73(Å)$^{-1}$. Eq. (4) in form of eq.(2) provides c = 2.681Å, and ln d =16.01. This eq. (4) in form of eq. (3) gives k = 16.01 and l. = 3.730 (Å)$^{-1}$.

From the eq. (2) to (4), the least square fitting was performed by Buanam-Om [22] for the data of $\nu_{OH}(HOD)$, $\nu_{OD}(HOD)$, and $R_{O...O}$ and reported the new correlation between $R_{O...O}$ and ln ($\Delta\nu_{OH}$/cm^{-1}), and $R_{O...O}$ and ln ($\Delta\nu_{OD}$/cm^{-1}). The results are illustrated in the following section.

2.5 The Relationship between ν_{OH} (HOD) or ν_{OD}(HOD) and $R_{O...O}$

The correlations between $R_{O...O}$ and ν_{OH} or ν_{OD} of the single OH and OD oscillator as a function of the O...O distance were described by Buanam-Om [22], as shown in eq. 5 and 6. The correlations of $\nu_{OH}(HOD)$ were carried out for crystalline hydrates and ices and have the forms of eq.5, while the correlation between $\nu_{OD}(HOD)$ and $R_{O...O}$ is shown in eq.6.

$$R_{O...O} = 4.105(Å) - 0.2201(Å)\ln(\Delta\nu_{OH}/cm^{-1}); \Delta\nu_{OH} = 3707 - \nu_{OH, Obs}(HOD) \ cm^{-1} ...(5)$$

$$R_{O...O} = 4.120(Å) - 0.2371(Å)\ln(\Delta\nu_{OD}/cm^{-1}); \Delta\nu_{OD} = 2727 - \nu_{OD, Obs}(HOD) \ cm^{-1}...(6)$$
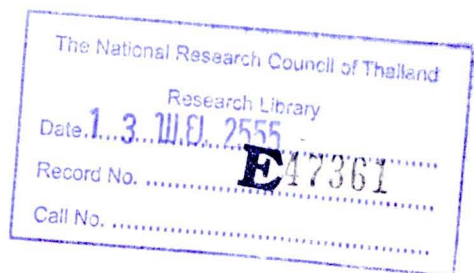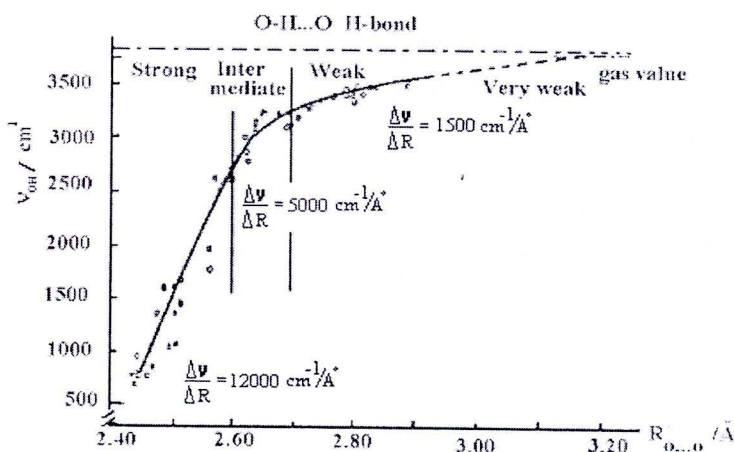
Figure 2.6 Correlation of uncoupled ν_{OH} band position (cm^{-1}) with O...O Distances [39,40].

Correlation equation reported in the literatures can be simplified and given in the form:

$$R_{O...O}(\text{Å}) = a\,(\text{Å}) - b(\text{Å}) \ln (\Delta\nu_{OH}/\text{cm}^{-1}) \qquad \ldots(7)$$

2.6   Correlation between ν_{OH}(HOD) and ΔH_H and Badger-Bauer Rule

Direct proportionality between frequency shift $\Delta\nu$ and H-bond energy becomes a conventional assumption in the H-bond spectroscopy [27]. The first experimental indication for $\Delta\nu \propto \Delta H$ was given by Badger and Bauer [41]. Luck demonstrated the validity of this relation for pyrrolidine with different proton acceptors. For system of phenol $\Delta\nu \sim \Delta H$ is approximately true. Reexamination of the so-call Badger-Bauer rule was done by Rao et al [4]. Theoretical aspects of this rule were treated by Purcell and Drago [43]. So far the relation, $\Delta\nu \propto \Delta H$ is true only for the same homologous series. General linear relation, $\Delta\nu = a \Delta H + b$ was found.[31,46]

The deuterated analogue of hydrates have been studied by using infrared and Raman spectroscopy by observing uncoupled ν_{OH}(HOD) in all techniques. The uncoupled ν_{OH}(HOD) values lead to the estimation of ΔH_H from following equation.

$$-\Delta H_H = 1.286 + 0.0418 \, (\Delta v_{OH}(HOD)/\,cm^{-1}) \qquad kJmol^{-1}OH \qquad ...(8)$$

This equation has been presented by Danvirutai and Jeradipalang [22, 44].

2.7   Vibrational Spectroscopic Studies of Crystalline Hydrates

Vibrational spectroscopies (IR and Raman) are known to be a powerful method for investigating hydrogen bonding and the structure of aquo systems [45]. In solid state, the vibrational spectra of molecular or ionic units are changed with respect to the gas or liquid phase. Bands may be:

(1)   increased in half width (in part strongly),

(2)   shifted to higher or lower wavenumbers,

(3)   additional bands, not allowed in the case of free molecules, may be observed,

(4)   split into two or more components, and further.

Thus, various normal modes of polyatomic units are mostly shifted to higher or lower frequencies. The following reasons are possible:

(1)   change of the polarity or the nature of the intramolecular bond, which may lead to a blue shift or red shift of the normal modes,

(2)   repulsive forces of the lattice, which cause only small blue shift,

(3)   weakening of the intramolecular bonds owing to intermolecular bonding features, which result in a red shift of the band as a consequence of the decrease of the respective internal force constant,

(4)   intermolecular coupling of normal modes which can produce both red shift and blue shift,

(5)   increase of the anharmonicity of vibrations, especially in the case of XH stretching modes of hydrogen bonded entities, which strongly enlarges the red shift as it is because of the weakening of the XH bond[46-48].

Vibrational spectroscopic studies of water in crystalline hydrate have been extensively studied, but the information from energetic point of view is lacking. Therefore, as well known that hydrates are suitable for studying ion-water, especially anion-water interaction.

The vibrations of equivalent water molecules in crystal may engage in dynamic coupling. The occurrence of such coupling represents a major complication in the interpretation of spectra of crystalline hydrates. Interpretation of vibrational spectra of water in hydrates is much simplified by using the isotopic dilution technique.

2.7.1 Vibrational Modes of Water Molecules in Solid Hydrates

A free H_2O molecule belongs to the C_{2v} point group and possesses three normal modes of vibration, namely $v_1(A_1)$, $v_2(A_1)$ and $v_3(B_2)$ of which v_1 and v_3 are stretching and v_2 is bending vibrations. In solid hydrates, there are in addition, the external H_2O librations (hindered rotation) (Figure 2.7) and H_2O translatory modes. Vibrational band positions of water in solid hydrates and free water molecule were reported as shown in Tables 2.2 and 2.3, respectively [10, 49].
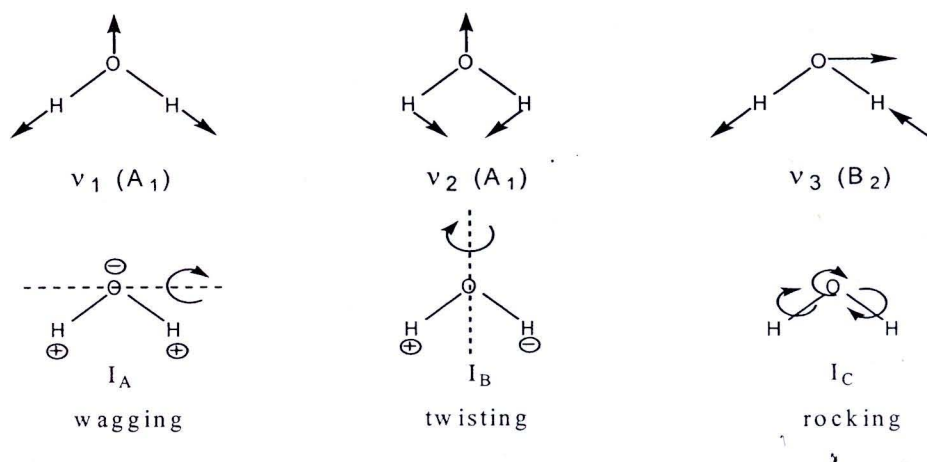
Figure 2.7 Vibrational modes (internal modes) and librational modes of a water molecule [49].

2.7.2 OH Stretching Vibrations

The stretching modes of water in solid hydrates are shifted to lower wavenumbers compared to those of free H_2O molecules for all compounds studied so far [50]. Furthermore, the intensities and halfwidths of the respective IR and Raman bands alter characteristically. These observations support the sensitivity of the stretching mode engaged in hydrogen bonding.

To prevent the intramolecular and intermolecular couplings, isotope dilution of about 5% has been widely used. The spectra of isotopically dilute samples mainly exhibit the following information:

(1) Strength and arrangement of hydrogen bonds and other intermolecular interactions.

(2) Number of different hydrogen position (OH oscillators) in the structure.

(3) Distortion of the water molecules and distortion of the hydrogen atom containing bonds.

The assignment of the two stretching modes is the same as for free water molecules, i.e., the symmetric mode (v_1) which is found at lower wavenumbers than the antisymmetric one (v_3) as far as intermolecular coupling of the two OH vibrations occurs. However, there is evidence that the assignment of these modes must be reversed, i.e., $v_1 > v_3$ for compounds with very strong H – bonds [51].

Table 2.2 Vibrational band position ranges (cm^{-1}) of the water in hydrates [49]

Solid hydrate	H_2O	HDO	D_2O
Stretching modes (v_1, v_3)	3600 - 3000	2600 - 2300	2650 - 2300
Bending mode (v_2)	1600 - 1590	1460 - 1400	1225 - 1175
Librations (ρ)	900 - 50	900 - 260	680 - 260
Translatory modes (T′)	350 - 100	-	330 - 95
(or Metal-O stretching mode)			

Table 2.3 Vibrational band position (cm^{-1}) of the H_2O, D_2O and HDO molecules [49]

Free molecules	$v_1(v_{sym})$	v_2	$v_3(v_{asym})$
Harmonic (ω_e)			
H_2O	3832	1648	3943
HDO	2824	1441	3890
D_2O	2764	1206	2889
Observed (ω_e)			
H_2O	3657	1595	3756
HDO	2727	1403	3707
D_2O	2671	1178	2788

2.7.3 H_2O Bending Vibration

Falk [30] described that, the structural factors influencing the frequency of the bending fundamental are as following.

(1)   Hydrogen bonding may be expected to provide an additional force resisting the H-O-H bending motion, thus raising v_2.

(2)   Dynamic coupling of bending vibrations of neighboring water molecules; this effect diminishes rapidly with increasing H_2O-H_2O distance and would be expected to be greatest for ices and those higher hydrates in which the water molecules are directly connected by hydrogen bond.

(3)   Interaction of the lone pairs with medium; this effect would be especially important in the case of water-cation coordination. The magnitude and sign of shifts of $v_2(H_2O)$ induce by cations are uncertain. Theoretical studies have shown that $v_2(H_2O)$ is raised; but some observation of spectra of aqueous electrolyte solution seem to indicate that $v_2(H_2O)$ is lowered by cations, while other observations point to no cation effect at all.

The bending mode $v_2(A_1)$ of the water molecule in solid hydrates is mostly observed in the relatively small spectral range from 1590 to 1660 cm^{-1}. The highest and lowest wavenumbers are found at 1721 and 1582 cm^{-1}, respectively[52].

appears at a lower wavenumber (appreciably lower than in gaseous water) in several solid hydrates. However, it is generally believed (very often found) that the water bending frequency is higher than that in gaseous water where it was found at 1594 cm^{-1}.

2.7.4 H₂O Librations

The water libration has three normal modes, the wagging (ρ_w), rocking (ρ_r) and twisting (ρ_t) (as shown in Figure 2.7). These modes in crystals present interesting problem in relation to IR spectroscopy, nuclear quadrupole resonance, etc., especially when water molecules are involved in the formation of hydrogen bonds.

The frequency of the librational band decreases in the order: $\rho_w > \rho_t > \rho_r$, for the water molecules in the tetrahedral surrounding (trivalent cation coordination) and the intensity sequence should be: $\rho_w > \rho_r > \rho_t$. In a trigonal surrounding of water (univalent cation coordination) the frequency should be in the order of $\rho_t > \rho_w > \rho_r$ and the intensity sequence should be $\rho_w > \rho_r > \rho_t$ [59-61].

2.8 Phosphate Ion (PO₄³⁻)

The normal mode of vibrations of PO_4^{3-} group comparision with HPO_4^{2-}, $H_2PO_4^{2-}$ and H_3PO_4 are illustrated in Table 2.4, which were derived by the site group method of Halfold. The fundamental normal vibrations (ν_1, ν_2, ν_3 and ν_4) of the free PO_4^{3-} ion are correlated with its vibrations in the crystal. The free tetrahedral (T_d) PO_4^{3-} ion has four normal modes of vibration. They are $\nu_1(A_1)$ symmetric stretching; ν_3 (F_2) asymmetric stretching; ν_4 (F_2) and ν_2 (E) bending vibrations. All four modes are Raman active, whereas only ν_3 (asymmetric stretching) and ν_4 (the out-of plane bending) are IR active. The ν_3 and ν_4 modes are triply degenerate, ν_2 is doubly degenerate and ν_1 is non-degenerate mode[62].

The spectra, together with published Raman data, are assigned on the basis of changes in symmetry through the series PO_4^{3-} (T_d), HPO_4^{2-} (pseudo C_{3v}) and $H_2PO_4^{-}$ (pseudo C_{2v}). Four fundamental modes of the free phosphate ion undergo factor group splitting. The O-H stretching of the HPO_4^{2-} and $H_2PO_4^{-}$ ions gives rise to a complex feature of which only the two former components are clearly visible, the third

component possibly contributing to the breath of the bands in the water bending region (1850-1495 cm^{-1}) and/or the multiple bands in this region. The origin of subsidiary or double OH stretching bands will be discussed. Bands in the region of 2300-2400 cm^{-1} (1750-1850 cm^{-1} in deuterated compounds) are attributed to proton-tunneling effect; band in the 1600-1850 cm^{-1} region probably arise from combination tones. The P-O-H in and out of plane deformation mode absorbs in the region of 1250 cm^{-1} and 860 cm^{-1}. These bands are typical characteristic of the HPO_4^{2-} and $H_2PO_4^{-}$ ions. The normal modes of vibration of PO_4^{3-} (T_d), HPO_4^{2-} (pseudo C_{3v}) and $H_2PO_4^{-}$ (pseudo C_{2v}) ions are shown in Table 2.4 and Figure 2.8, respectively.
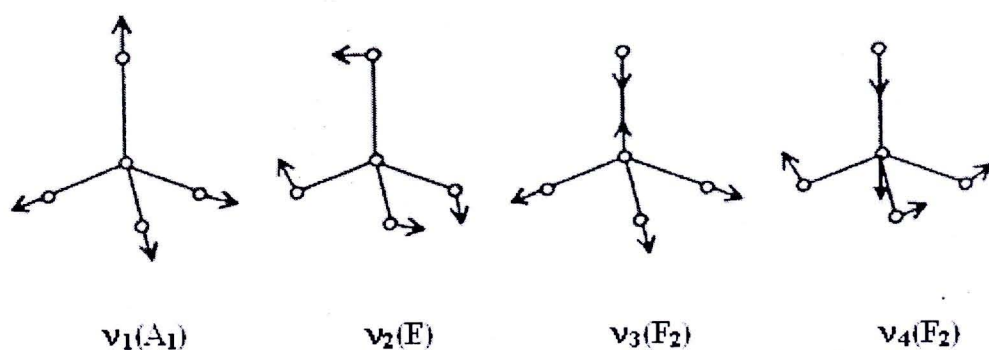

$$\nu_1(A_1) \qquad \nu_2(E) \qquad \nu_3(F_2) \qquad \nu_4(F_2)$$

Figure 2.8 Normal modes of vibration of PO_4^{3-} (T_d) ion [63].

Table 2.4 The vibrational frequencies of PO_4^{3-}, HPO_4^{2-}, $H_2PO_4^-$ and H_3PO_4 (cm^{-1})

Free ion	Symmetry species	Band position (cm^{-1})	Assignment
	(T_d Point group)		
PO_4^{3-}	F_2	1010	$\nu_3(F_2)PO_4^{3-}$ or ν_{as}(P-O)
(T_d)	A_1	934	$\nu_1(A_1)PO_4^{3-}$ or ν_s(P-O)
	F_2	567	$\nu_4(F_2)PO_4^{3-}$ or δ(O-P-O)
	E	420	$\nu_2(E)PO_4^{3-}$ or δ(O-P-O)
	(C_{3v} Point group)		
	E	1077	$\nu_3(F_2)PO_4^{3-}$ or ν_{as}(P-O)
HPO_4^{2-}	A_1	989	$\nu_1(F_2)PO_4^{3-}$ or ν_s(P-O)
(pseudo C_{3v})	A_1	847	$\nu_3(A_1)PO_4^{3-}$ or ν_s(P-OH)
	E	580	$\nu_2(F_2)PO_4^{3-}$ or δ(O-P-O)
	A_1	535	$\nu_4(F_2)PO_4^{3-}$ or δ(O-P-O)
	E	394	$\nu_2(E)PO_4^{3-}$ or δ(P-OH)
	(C_{2v} Point group)		
	A_1	1155	$\nu_3(F_2)PO_4^{3-}$ or ν_s(P-O)
	B_1	1075	$\nu_3(F_2)PO_4^{3-}$ or ν_{as}(P-O)
$H_2PO_4^-$	B_2	940	$\nu_3(F_2)PO_4^{3-}$ or ν_{as}(P-OH)
(C_{2v} or lower)	A_1	874	$\nu_1(A_1)PO_4^{3-}$ or ν_s(P-OH)
	A_1	567	$\nu_4(F_2)PO_4^{3-}$ or δ(O-P-O)
	B_2	540	$\nu_4(F_2)PO_4^{3-}$ or δ(P-O$_2$)
	B_1	527	$\nu_4(F_2)PO_4^{3-}$ or δ(P-O$_2$)
	A_2	510	$\nu_2(E) PO_4^{3-}$ or δ(P-O$_2$)
	A_1	380	$\nu_2(E)PO_4^{3-}$ or δ(HO-P-OH)

Table 2.4 The vibrational frequencies of PO_4^{3-}, HPO_4^{2-}, $H_2PO_4^-$ and H_3PO_4 (cm^{-1}) (Cont.)

Free ion	Symmetry species	Band position (cm^{-1})	Assignment
	(C_{3v} Point group)	1174	$v_3(F_2)PO_4^{3-}$ or v_s(P=O)
H_3PO_4	A_1	1106	$v_3(F_2)PO_4^{3-}$ or v_{as}(P-OH)
(lower than pseudo C_{3v})	E	890	$v_1(A_1)PO_4^{3-}$ or v_s(P-OH)
	A_1	500	$v_4(F_2)PO_4^{3-}$ or δ(HO-P-OH)
	E	394	$v_4(E)PO_4^{3-}$ or δ(HO-P-OH)
	A_1	345	$v_2(E)PO_4^{3-}$ or δ(P-(OH)$_3$)
	E		

2.9 Experimental Techniques

Characterization techniques in this work are the elemental chemical analysis (AAS and AES), Karl Fischer coulometric titration, thermoanalytical techniques (DSC and TG/DTG/DTA), X-ray powder diffraction (XRD), Fourier transform infrared (FTIR) and Fourier transform Raman (FT Raman) spectroscopies.

2.9.1 X-Ray Powder Diffraction (XRD) Technique

A beam of X-rays passing through a sample of randomly-oriented microcrystals produces a diffracted X-ray pattern of ring on a distant screen. Powder X-ray diffraction provides less information than single-crystal diffraction, however, it is much simpler and faster. Powder X-ray diffraction is useful for confirming the identity of a solid material and determining crystallinity and phase purity. Diffraction techniques exploit the scattering of radiation from large numbers of site. There are various diffraction techniques currently employed and the diffraction patterns are recorded. The interpretation from diffraction patterns are, for examples, the average spacing between layers or row of atoms, the orientation of a single crystal or grain,

the crystal structure of an unknown material as well as the size, shape and internal stress of small crystalline regions.

In this work, the X-ray diffraction (XRD) patterns are interpreted to confirm the identity of the prepared phosphate compounds by comparing with the standard PDF database for chemical identification. Cell parameters are obtained from a least square refinement of the XRD data with the aid of a computer program corrected for systematic experimental errors. Crystallite size (D) was calculated using Scherrer equation:

$$D = \frac{k\lambda}{\beta \cos\theta} \qquad \qquad ...(9)$$

where λ is the wavelength of X-ray radiation (Cu K_α, $\lambda = 1.5406$ Å), k is a constant taken as 0.89, θ is the diffraction angle and β is the full width at half maximum (FWHM) [64-65].

2.9.2 Atomic Absorption Spectroscopy (AAS)

Atomic absorption spectroscopy (AAS) as shown in Figure 2.9 uses the absorption of light to measure the concentration of gas-phase atoms. Since samples are usually solids, the analyte atoms or ions must be vaporized in a flame or graphite furnace. The atoms absorb ultraviolet or visible light and make a transition to higher electronic energy levels. The analyte concentration is determined from the amount of absorption. Applying the Beer-Lambert law directly in AA spectroscopy is difficult due to variations in the atomization efficiency from the sample matrix, and non uniformity of concentration and path length of analyte atoms (in graphite furnace AA). Concentration measurements are usually determined from a working curve after calibrating the instrument with standards of known concentration.
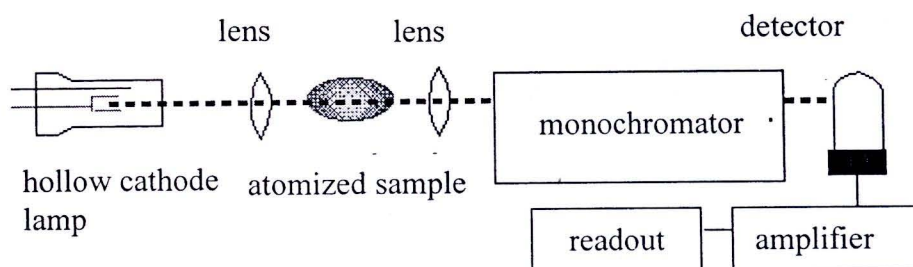
Figure 2.9 Block diagram of atomic absorption spectrophotometer (AAS).

Instrumentation

Light Source

The light source is usually a hollow-cathode lamp of the element that is being measured. Lasers are also used in research instruments, since lasers are intense enough to excite atoms to higher energy levels, they allow AA and atomic fluorescence measurements in a single instrument. The disadvantage of these narrow-band light source is that only one element is measurable at a time [66].

Atomizer

AA spectroscopy requires that the analyte atoms must be in the gas phase. Ions or atoms in a sample must undergo desolvation and vaporization in a higher-temperature source such as a flame or graphite furnace. Flame AA can only analyze solutions, while graphite furnace AA can accept solutions, slurries, or solid samples. Flame AA uses a slot type burner to increase the path length, and therefore to increase the total absorbance base on Beer-Lambert law. Sample solutions are usually aspirated with the gas flow into a nebulizing/mixing chamber to form small droplets before entering the flame. The graphite furnace has several advantages over a flame. It is a much more efficient atomizer than a flame and it can directly accept very small absolute quantities of sample. It also provides a reducing environment for easily oxidized elements. Samples are placed directly in the graphite furnace and furnace is electrically heated in several steps to dry the sample, ash organic matter, and vaporize the analyze atoms.

Light Separation and Detection

AA spectrometers use monochromators and detectors for UV and visible light. The main purpose of the monochromators is to isolate the absorption line from background light due to interferences. Simple dedicated AA instruments often replace the monochromator with a band pass interference filter. Photomultiplier tubes are the most common detectors for AA spectroscopy.

2.9.3 Atomic Emission Spectroscopy (AES)

The block diagram of this instrumentation is as nearly the same as the atomic absorption technique, however , the position of excitation source differs from the AA technique as illustrated in Figure 2.10.
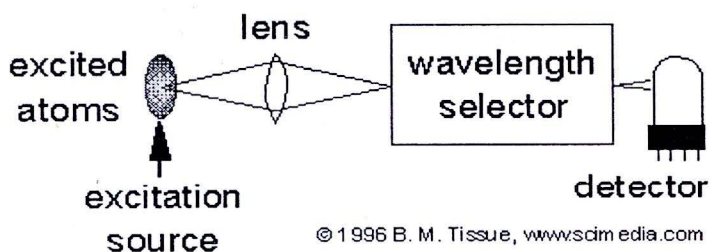

**Figure 2.10** Block diagram of atomic emission spectrophotometer (AES).

2.9.4 Karl Fischer Technique

Karl Fischer (KF) titration is a widely used analytical method for quantifying water content in a variety of products. The fundamental principle behind is based on the Bunsen reaction between iodine and sulfur dioxide in an aqueous medium. Karl Fischer discovered that this reaction could be modified to be also used to determine the water contents in a non-aqueous system containing an excess of sulfur dioxide. This study, a primary alcohol (methanol) as the solvent, and a pyridine base as the buffering agent (reaction with the acidic products, H_2SO_4) [67].

Several products as well as solvents and raw materials are analyzed for their water content (or % humidity). Of all the available methods, the Karl Fischer procedure is the most widely used.

26

This type of analysis is conducted with dedicated instruments. It uses chemical reactions that resemble to the electrochemical detection. The determination can be carried out in two different ways. The first is conducted in classical way using titration and the second is a coulometric method using a diaphragm cell. The latter is the more sensitive one, which can be applied to the determination of very low level of water (in the order of mg/L) including hydrates [68].

In the presence of water, iodine reacts with sulphur dioxide through a redox process, that is specific to the three compounds present:

$$I_2 + SO_2 + 2H_2O \xrightarrow{\quad C_5H_5N,\ CH_3OH \quad} 2HI + H_2SO_4 \qquad ...(10)$$
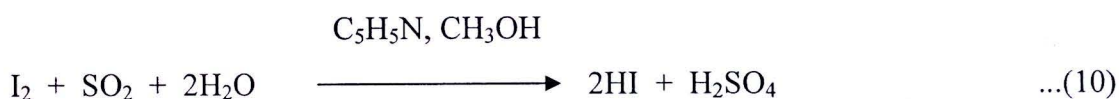
This reaction can be used to determine water if the transformation is stoichiometric. This is why a base is added to the reaction medium to neutralize the acid formed (pyridine is traditionally used in the Karl Fischer method).

Since iodine is a solid and sulphur dioxide is a gas, a polar solvent must be used for the reaction and as a dilution agent. Methanol is generally used as the solvent; however, it can be replaced by methylmonoether glycol or diethylene glycol. In these conditions, sulphur dioxide is not simply dissolved in the solvent but actually interacts with it. For example, with methanol, SO_2 is transformed into methylhydrogen sulphite (CH_3OSO_2H) that reacts with I_2 in the presence of water as follow:

$$CH_3OSO_2H + I_2 + H_2O \rightleftharpoons CH_3OSO_3H + 2HI \qquad ...(11)$$

In contrast to the previous reaction, in this case a single molecule of water reacts with one molecule of iodine. Methylhydrogen sulphite is oxidized to methyl hydrogensulphate, which is converted in the presence of a base of type RN into an ammonium salt. The Karl Fischer reaction can thus be reformulated as follows:

$$H_2O + I_2 + [RNH]^+ CH_3OSO_2^- + 2RN \longrightarrow 2[RNH]^+I^- + [RNH]^+CH_3OSO_3^- \quad ...(12)$$

When pyridine is used as a base, a pyridinium salt $C_5H_5NH^+ (CH_3OSO_3)^-$ is formed. Nowadays, pyridine is replaced by imidazole or diethanolamine, which are stable and less odorous commercial products.

Because atmospheric humidity must be avoided, the reaction flask is isolated from atmosphere with drying tubes. Moreover, since the solvent is rarely perfectly anhydrous and will be containing traces of water due to its hygroscopic nature, its water content must be measured prior to the determination. The equivalent point of the titration reaction is detected by an electrical method instead of a visual method. The current intensity that passes between two platinum electrodes inserted in the reaction medium is measured. The reagent, which is mixture of sulphur dioxide, iodine, and a base, is characterized by the number of milligram of water that can be completely reacted by 1 mL of KF reagent. This is refered to as the equivalent mass concentration of water, or the titer (T) of the reagent. The block diagram of this instrumentation illustrated in Figure 2.11.
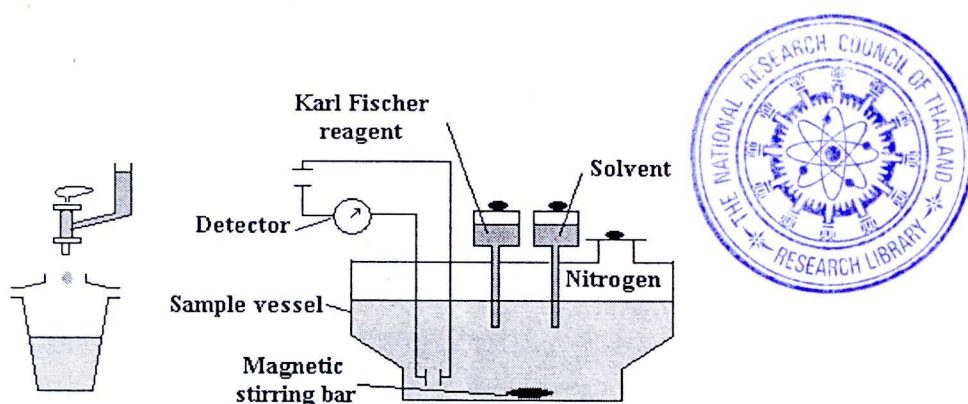

Figure 2.11 Karl Fischer method for determination of water. The conventional
burette titration with visual detection of the end point to imprecise
results. Thus, a cell containing two small platinum electrodes is used.
As long as no iodine is present in the solution, the current between
the electrodes is weak. When excess iodine is present in the solution
the equivalence point is reached, a significant current is registered.

2.9.5 Vibrational Spectroscopy

Molecules consist of atoms which have a certain mass and are connected by elastic bonds. As a result, they can perform periodic motions of a certain number of vibrational degree of freedom. All motions of the atoms in molecule relative to each other are a superposition of so called normal vibration, in which all atoms are vibrating with the same phase and normal frequency. Their amplitudes are described by a normal coordinate. Polyatomic molecules with N atom possess 3N-6 normal vibrations (linear ones have 3N-5 normal vibrations), which determine their vibrational spectra. The spectra depend on the masses of the atoms, their geometrical arrangements, and the strength of their chemical bonds [71]. Raman and Infrared spectrometers are the most important tools for observing vibrational spectra. The symmetry of the molecules is an important nature to determine the vibrations whether they are active or forbidden in the infrared as well as Raman spectrum.

Infrared Spectroscopy

Infrared spectra are usually recorded by measuring the transmittance of light quanta with a continuous distribution of the sample. The frequencies of the absorption bands v_s are equal to the energy difference between the vibrational ground and excited states (Figure 2.12). The absorption bands due to the vibrational transition are found in the wavelength region of 2.5-1000 μm or in the wavenumber range of 4000-10 cm^{-1}.

IR absorption band positions are generally presented as either wavenumber (v) or wavelengths (λ). Wavenumber defines the number of wave per unit length. Thus, wavenumbers are directly proportional to frequency as well as the energy of the IR absorption. IR absorption information is generally presented in the form of a spectrum with wavelength or wavenumber in the x-axis and the absorbance (absorption intensity) or percent transmittance in the y-axis. The IR region is commonly divided into three subareas: near IR, middle IR (fundamental) and far IR.
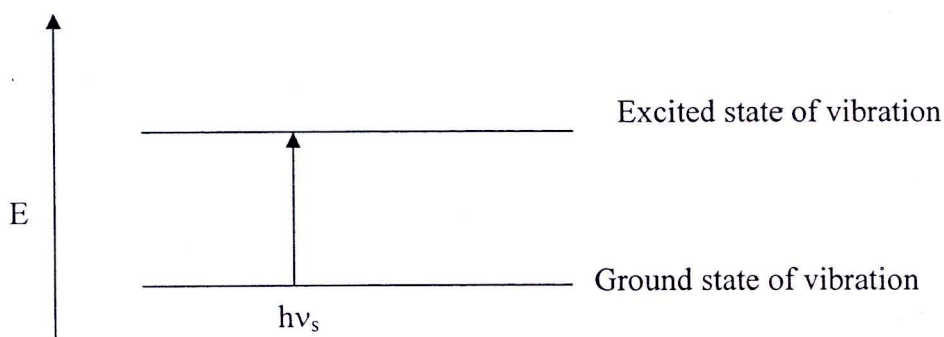
Figure 2.12   Diagram of principle infrared absorption.

Raman Spectroscopy

Raman Spectroscopy is the measurement of the wavenumber versus intensity of inelastically scattered light from molecules. The Raman scattered light occurs at wavenumber or frequency that is shifted from the incident light by the energies of molecular vibrations. The mechanism of Raman scattering is different from that of infrared absorption. Therefore, Raman and IR spectra provide complementary information. Typical applications are in structure determination multicomponent qualitative analysis, and quantitative analysis [71]. The principle of this technique is illustrated in Figure 2.13.

Figure 2.13, consider a light wave as a stream of photons each with energy $h\nu$. When each photon collides with a molecule, two processes can occur. Firstly, an elastic scattering or Rayleigh scattering (Figure 2.13 a). The collision between photon and a molecule do not exchange the energy. The vast majority of photons will be scattered in this way. Secondly, the collision undergoes inelastic collision or Raman scattering (Figure 2.13 b).

There is an exchange of energy between the photon and the molecule, leading to the emission of another photon with a different frequency to the incident photon. This scattering can be subdivided into two types. If the molecule relaxes to energy state E_1, it loses the energy, and so the photon emits with the energy $h\nu_1$, where $h\nu_1 > h\nu$. These transitions are known as anti-Stokes transitions. If the molecule relaxes to energy state E_3, it gains the energy, and so the emitted photon has the energy of $h\nu_2$, where $h\nu_2 < h\nu$. These transitions are known as Stokes transitions.
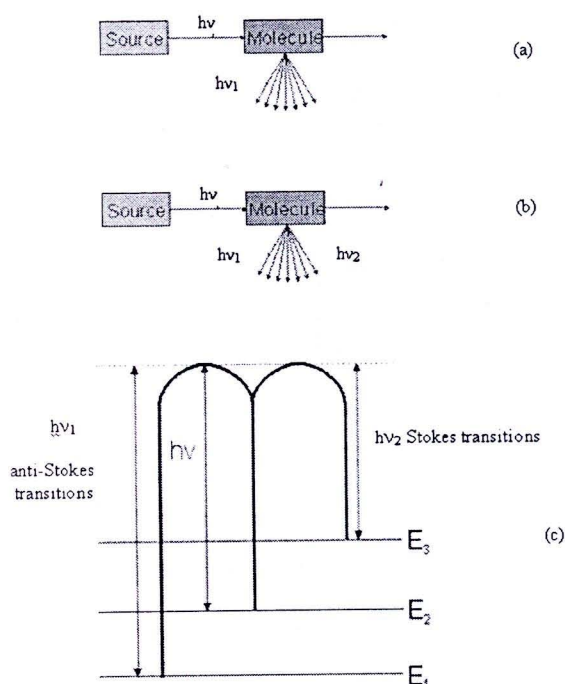
Figure 2.13 Principle of Raman spectroscopy (a) Elastic, or Rayleigh scattering (b) Inelastic, or Raman scattering (c) Anti-Stokes and Stokes transition [74].

2.10 Thermal Analysis Techniques

Thermal analysis (TA) comprises a group of techniques in which a physical property of the substance is measured as a function of temperature, while the substance is subjected to a controlled temperature programme. Thermal analysis, in its various guises, is widely employed in both scientific and industrial domains. The ability of these techniques to characterize, quantitatively and qualitatively, a huge variety of materials over a considerable temperature range has been pivotal in their acceptance as analytical techniques.

Thermal analysis refers to conventional thermal analysis techniques such as differential scanning calorimetry (DSC), differential thermal analysis (DTA), thermogravimetry (TG). In this work, the selected hydrates are characterized by differential scanning calorimetry (DSC) and thermogravimetry and differential thermal analysis (TG/DTA).

2.10.1 Thermogravimetry (TG) [75]

Thermogravimetry (TG) is the branch of thermal analysis which examines the mass change of a sample as a function of temperature in the scanning mode or as a function of time in the isothermal mode (Hatakeyama & Quinn, 1999). TG is used to characterize the composition and thermal stability of materials under a variety of condition and to examine the kinetics of the physicochemical process occurring in the sample. The mass change characteristics of a material are strongly dependent on the experimental conditions employed. Factors such as sample mass, volume and physical form, the shape and nature of the sample holder, the nature and pressure of the atmosphere in the sample chamber and the scanning rate all have important influenced on the characteristics of the recorded TG curve.

TG cannot be considered as a box technique where fingerprint curves are obtained irrespective of the experimental conditions. Establishing the optimum conditions for TG analysis frequently requires many preliminary tests. It is essential for accurate TG work that the experimental conditions be recorded and that within a given series of samples the optimum condition be standardized and maintained throughout the course of the experiments. Only then can TG curves from different experiments be compared in a meaningful way.

TG curves are normally plotted with the mass change (Δm) expressed as a percentage on the vertical axis and temperature (T) or time (t) on the horizontal axis. A schematic representation of a one – stage reaction process observed in the scanning mode is shown in Figure. 2.14
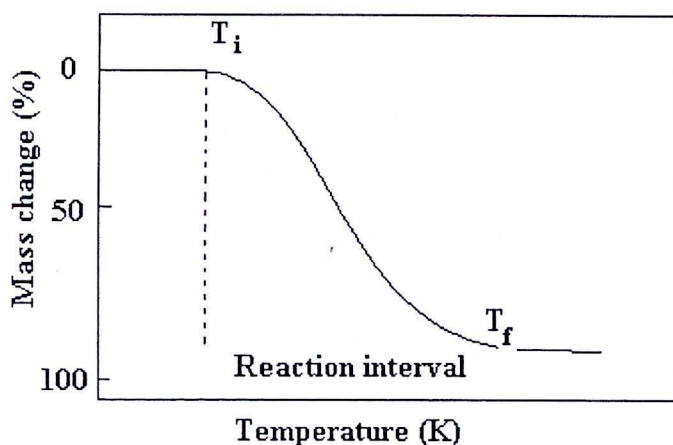

Figure 2.14 Schematic single – stage TG curve.

The reaction is characterized by two temperatures, T_i and T_f, which are called the procedural decomposition temperature and the final temperature, respectively. T_i merely represents the lowest temperature at which the onset of a mass change can be detected for a given set of experimental conditions. Similarly, T_f represents the lowest temperature by which the process responsible for the mass change has been completed. The values of T_i and T_f have no absolute significance as both the reaction temperature and the reaction interval $(T_i - T_f)$ have no definitive value but depend on the experimental conditions.

Interpretation of TG data is often facilitated by comparison with data from other experimental techniques. Many TA instrument manufactures offer simultaneous TG – DTA apparatus. The advantage of simultaneous apparatus is that the sample and experimental conditions are identical, and therefore directly comparative data can be quickly obtained. However, the performance of one or both components may be compromised in a simultaneous apparatus owing to the contrasting design features of the instruments.

2.10.2 Differential Thermal Gravimetric Analysis (DTG) [76]

In conventional thermogravimetry, the mass of a sample, m, is continuously recorded as a function of temperature (T) or time (t).

$$m = f(T \text{ or } t) \qquad , \qquad \ldots(13)$$

Quantitative measurements of the mass-changes are possible by determination of the distance, on the curve mass axis, between the two points of interest or between the two horizontal mass levels. In derivative, dm/dt, is recorded as a function of temperature or time. That means:

$$dm/dt = f(T \text{ or } t) \qquad \ldots(14)$$

2.10.3 Differential Thermal Analysis

Differential thermal analysis (DTA) is the most widely known technique of thermal analysis, and is useful for studying endothermic or exothermic phenomena (such as transition, chemical reaction, adsorption, etc.) occurring on

substances, materials and systems. In DTA, the difference in temperature (ΔT) between the sample and reference material is measured while both are subjected to the same temperature program. The temperature changes in the sample are due to endothermic or exothermic enthalpic transition or reaction such as those causes phase changes, fusion, crystalline structure inversions, boiling, sublimation, and vaporization, dehydration reaction, dissociation or decomposition reaction, oxidation and reductions reaction, destruction of crystalline lattice structure, and other chemical reactions. Generally speaking, crystallization, oxidation, and some decomposition reactions produce exothermal effect, whereas phase transitions, dehydration, reduction, and some decomposition reactions produce endothermic effects.

DTA involves heating or cooling a test sample and an inert reference under identical conditions, while recording any temperature difference between the sample and reference (Bhadeshia, 2002). This differential temperature is then plotted against time, or against temperature. Changes in the sample which lead to the absorption or evolution of heat can be detected relative to the inert reference. The structure of a classic differential thermal analyser is illustrated in Figure. 2.15.
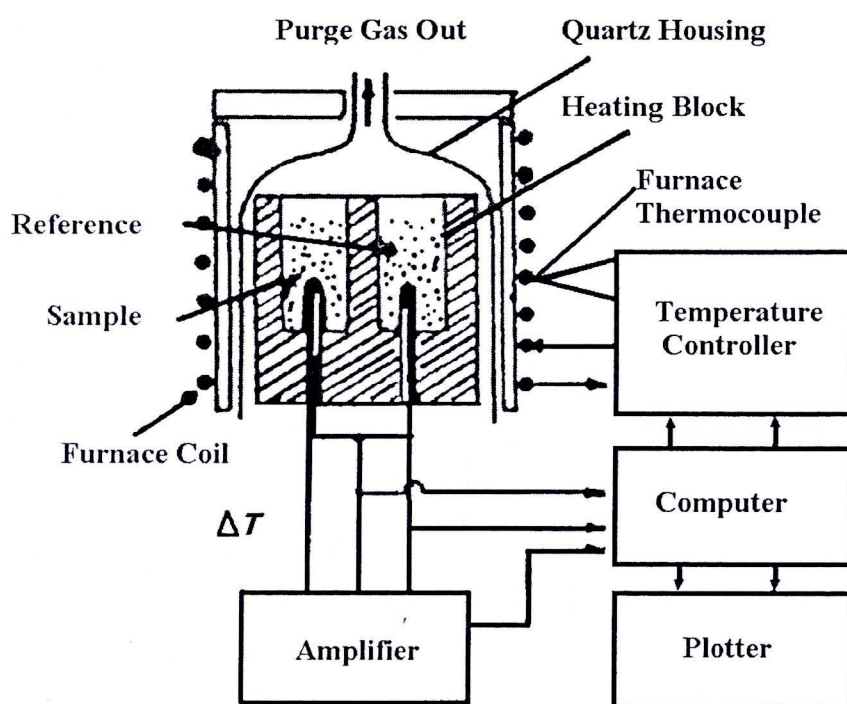

Figure 2.15 Schematic diagram of classical DTA apparatus
(Hatakeyama & Quinn, 1999).

A DTA curve plots the temperature difference as a function of temperature (scanning mode) or time (isotherm mode). During a phase transition the programmed temperature ramp cannot be maintained owing to heat absorption or emission by the sample. This situation is illustrated in Figure. 2.16, where the temperature of the sample holder increases above the programmed value during crystallization owing to the exothermic heat of crystallization.
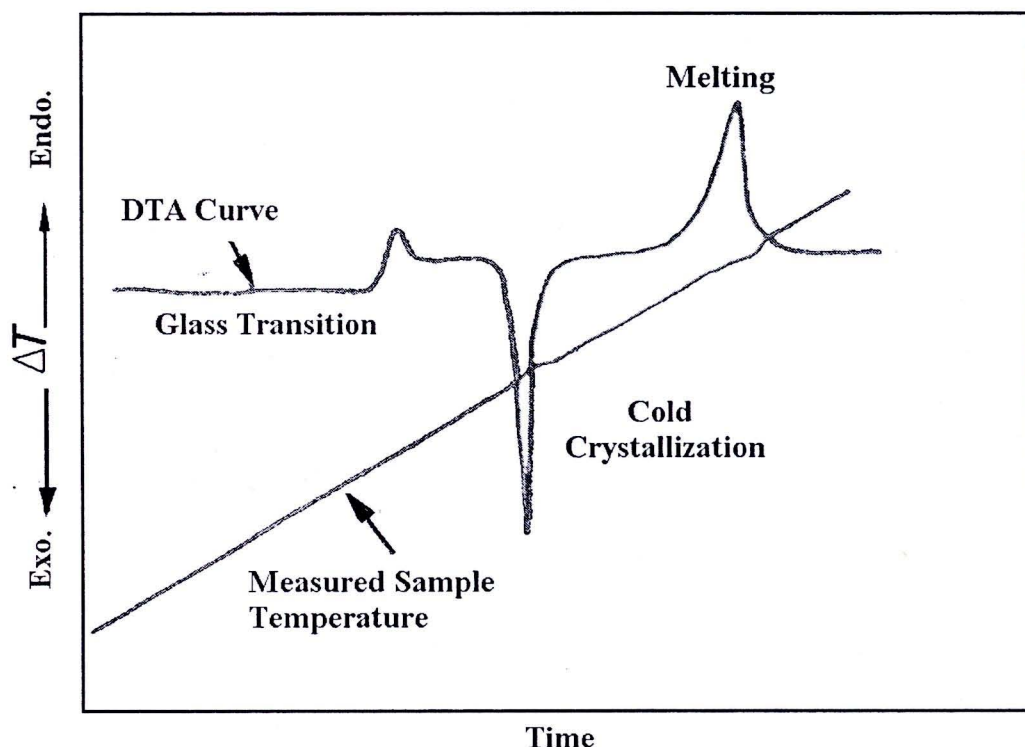

Figure 2.16 Schematic illustration of the measured sample temperature as a function of time for a polymer subjected to a linear heating ramp, and the corresponding DTA curve. In the region of the phase transitions the programmed and measured sample temperatures deviate significantly (Hatakeyama & Quinn, 1999).

In contrast, during melting point the temperature of the sample holder dose not increase in respond to the temperature programmer because heat flows form the sample holder to the sample. Therefore, the true temperature scanning rate of the sample is not constant over the entire temperature range of the experimental (Hatakeyama & Quinn, 1999).

2.10.4 Differential Scanning Calorimetry

Differential scanning calorimetry (DSC) has evolved from the technique of differential thermal analysis (DTA). There was no fundamental change in the measuring principle, only the position of the thermocouple sensors and controlling the transport of heat to the sample - keeping it at a nearly constant value - was improved by careful arrangement of the parts of the apparatus. A number of special solutions was applied in instrument design, which, however, will not be discussed here in detail.

The instrument used for DSC measurements can be divided into two groups, according to their basic principle of operation.
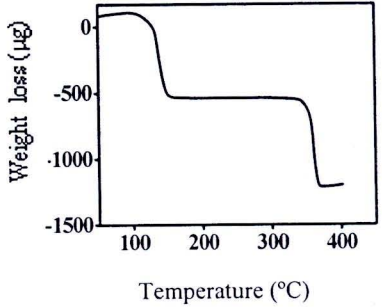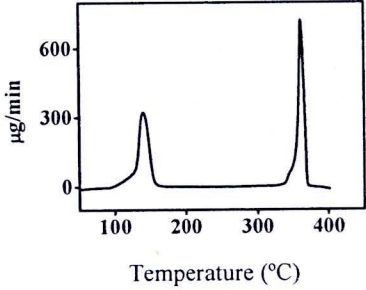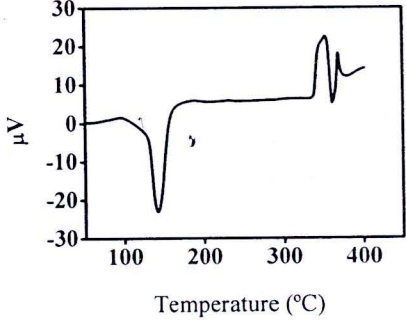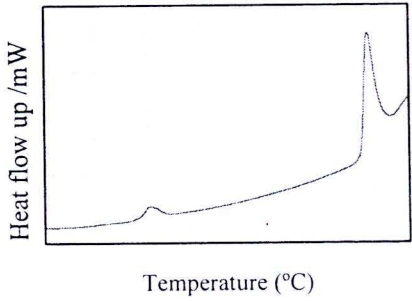
(1) The temperatures of the sample and of the reference material are kept at an identical value, while the temperature of the reference material is increased according to a program. The recorder records the increase in electric power necessary to attain this identity of temperatures, as a function of time. The integral of the curve recorded in the course of a transition gives the heat of transition. An apparatus working along this principle is manufactured by the firm Perkin-Elmer.

(2) The difference in the temperatures of the sample and the reference material are recorded (DTA principle) while the heat transport is controlled [70].

Two types of DSC systems in common use are heat flux DSC and power-compensation DSC (Figure 2.17). In heat flux DSC, the sample and reference are connected by a low resistance heat flow path (a metal disc). The assembly is enclosed in a single furnace. Enthalpy or heat capacity changes in the sample cause a difference in its temperature relative to the reference; the resulting heat flow is small compared with that in differential thermal analysis because the sample and reference are in good thermal contact. The temperature difference is recorded and related to enthalpy change in the sample using calibration experiment .

TG, DTG, DTA and DSC are known to be the thermal analysis techniques that are useful for solving chemical problems. The difference of principle of these techniques are described in Table 2.5.

Table 2.5   The differences of principles of TG, DTG, DTA and DSC techniques

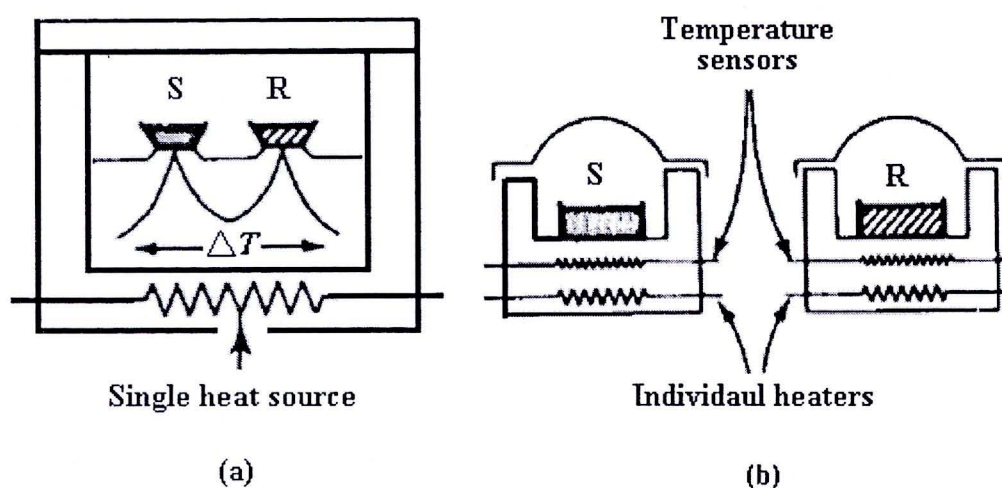| Technique	Parameter Measured	Instrument Employed	Typical Curve
Thermogravimetry (TG)	Mass	Thermobalance	
Derivative thermogravimetry (DTG)	dm/dt	Thermobalance	
Differential thermal analysis (DTA)	$T_S - T_R$ (ΔT)	DTA apparatus	
Differential scanning calorimetry (DSC)	Heat flow, dH/dt	DSC calorimeter	

Figure 2.17 Type of DSC; (a) Heat flux DSC and (b) Power – compensation DSC.

2.11 Isotope Dilution Technique

The isotope dilution technique has become a well-established method in solid hydrate research, especially for infrared and Raman studies. For this method, hydrates or deuterated hydrate samples containing small amount of HOD molecules matrix isolated in the bulk H_2O or D_2O are investigated. The main advantage of studying so called isotopically dilute sample is the fact that the vibrations of dilute HOD molecules do not exhibit any intramolecular and intermolecular couplings. The observed v_{OH} (HOD) or v_{OD} (HOD) is called an uncoupled vibration. Therefore, the OH and OD stretching frequencies of the dilute HOD molecules are a direct measure of the lattice potential in the various hydrogen position of the structure and hence the strength of H-bond[75,76].

Several isotopic effects are found that the frequency shifts on the deuteration are connected to the mass ratio. These isotopic effects are caused by the different vibrational zero point energies, the different tunneling probabilities, and the different strength of H-bonds of hydrates and deuterated hydrates [77].

The higher zero point energies and the larger strengths of H-bonds in the case of the non-deuterated compounds compared to the deuterated ones give rise to various structural hydrogen bond energies. Thus, the unit cell dimensions of deuterohydrates are somewhat larger than those of the non-deuterated specimens. The OD bond

lengths are smaller, and the OD⋯H distances are larger than the respective hydrogen distances (geometric isotope effect). However, geometric isotope effects are only observable in the case of strong H-bonds with O⋯O distance less than 2.70 Å, or hydrates with dynamical disorder of molecules. Further H/D isotopic effects are [61]:

(1)   the increased intensities and decreased halfwidths of D_2O (and HOD) bands compared to those of H_2O in both the Raman and infrared specra,

(2)   possible deviations from random distribution of H and D

in partially deuterated specimens, but the deuterium atom rather prefect those position which are involved in stronger H-bond.
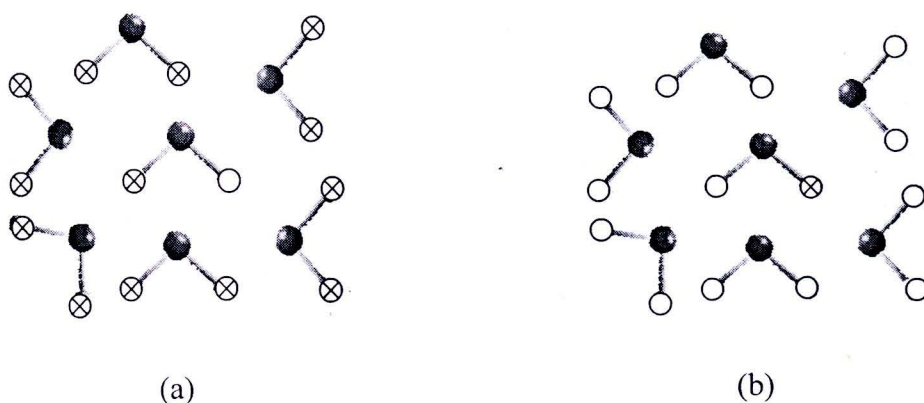

(a)   (b)

Figure 2.18   Coordination of HOD molecule in the D_2O surrounding (a) and H_2O surrounding (b) (● = O atom, ⊗ = D atom and ○ = H atom) [75,76].

2.12   Thermal Decomposition Kinetic Analysis

Phosphates transform to various forms of phosphates by hydrolysis and dehydration reaction. The formation and structure of phosphates depend on heating temperature, rate, time, cooling rate of melts, the atmosphere, kinds of cation in phosphate, and the ratio of phosphorus/cation. The ratio of phosphorus/cation varies in orthophosphate and various condensed phosphates. Thermal products depend severely on the ratio of phosphorus/cation [41].

Thermal treatment of inorganic phosphates has a great synthetic potential as it may turn simple compound into advanced materials, such as catalysts, ceramic

materials, fluorescent materials, dielectric substance, metal surface treatment, manure, detergent, food additive, fuel cells, dye pigments and glasses. The mechanism and kinetic studies of solid-state reactions are needed in order to take advantage of this potential [74-76].

Decomposition of solids is the subjects of intensive kinetics studies [78-80]. In many methods of kinetic estimation, isoconversional method is recommend as trustworthy way of obtaining reliable and consistent kinetic information [81]. The aim of the kinetic studies from TA data is to find the most probable kinetic model which gives the best description of the studied compound and allows the calculation of reliable values for the kinetic parameters (E_a and A). The kinetic parameters E_a and A together with the reaction model, are sometimes called the kinetic triplet.

In this work, model-free and model fitting approaches were used to investigate the kinetics under multiple-scan non-isothermal conditions. As one of the non-isothermal multiple-scan methods for studying of kinetics, isoconversion method is also called model-free method, because no kinetic model was set before the calculation of activation energy. Decomposition of crystalline hydrates is a solid-state process of the type:

$$A \text{ (solid)} \longrightarrow B \text{ (solid)} + C \text{ (gas)} \qquad ...(15)$$
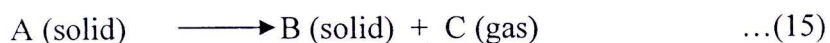
The kinetics of such reactions is described by various equations taking into account the special features of their mechanisms. The reaction rate can be expressed through the degree of conversion α (the ratio between the weight loss at the time t and the total weight loss at the end of dehydration). The temperature dependence of α is described as:

$$\frac{d\alpha}{dt} = k(T) \, f(\alpha) \qquad ...(16)$$

where t is the time, T is the temperature (K), α is the extent of conversion: $\alpha = (W_i - W_t) / (W_i - W_f)$; W_i, W_t and W_f are the initial, actual and final weights of the sample, respectively. The $f(\alpha)$ is the reaction model, which may take various

forms. The explicit temperature dependence of the rate constant is introduced by replacing k(T) from the Arrhenius equation ($k = A \exp(-E_a / RT)$), which gives,

$$\frac{d\alpha}{dT} = \frac{A}{\beta} \exp\left(\frac{-E_\alpha}{RT}\right) f(\alpha) \qquad \qquad ...(17)$$

where A (the pre-exponential factor/ s^{-1}) and E_α (the activation energy/ $kJmol^{-1}$) are the Arrhenius parameters, R is the gas constant (8.314 J mol^{-1} K^{-1}), $\beta = dT/dt$ is the heating rate. Under non-isothermal conditions in which a sample is heated at a constant rate, the explicit temperature dependence in eq. 17 is eliminated through the trivial transformation.

Calculation of Activation Energy

Ozawa method [82] and Kissinger method are two representative ones of model-free methods, which are convenient to calculate the activation energy [83], and take the following forms:

Ozawa equation:

$$\ln \beta = - \frac{E_a}{RT_m} + const \qquad \qquad ...(18)$$

Kissinger equation:

$$\ln \left(\frac{\beta}{T_m^2}\right) = - \frac{E_a}{RT_m} + const \qquad \qquad ...(19)$$

where β is the heating rate (°C min^{-1}), T_m is absolute maximum temperature on DSC curve (K), E_a is the activation energy of the process (kJ mol^{-1}), const are integration constants and R is the universal gas constant, 8.314 JK^{-1} mol^{-1}. Either the plot of $ln\beta$ versus $1000/T_m$ for Ozawa method or the plot of $ln (\beta/T_m^2)$ versus $1000/T_m$ for Kissinger method give a straight line from which the activation energy values for the processes are calculated from the slope.

Pre-exponential factor (A) was determined by using the following equation:

$$A = \frac{\beta E_a e^{E_a / RT_m}}{RT_m^2} \qquad \qquad ...(20)$$

2.13 Symmetry in Structural Chemistry

A knowledge of the symmetry concepts in chemistry affords one a better understanding of the ever-increasing battery of tools available for the solution of structural problems. Infrared, Raman and ultraviolet spectroscopy, and X-ray, electron, and neutron diffraction methods are some of the powerful tools that are based on symmetry consideration. Knowing the symmetry of a molecule, one can predict the infrared or Raman spectrum, and knowing the spectrum, one can arrive at symmetry or structure of the molecule. The details of symmetry in structural chemistry ; point groups, space group, site group and factor group are described in reference 79. Group theory can be used to determine the number of fundamental vibrations allowed in the Infrared and Raman spectrum [84]. To determine which fundamentals will be active in the infrared, the character of the dipole moment $\chi_M(R)$ is used where

$$\chi_M(R) = \pm 1 + 2\cos\psi \qquad \ldots(21)$$

The angle ψ is associated with the proper rotation. The negative sign is used with the improper rotation. The reduction formula :

$$N_i = 1/N_G \sum n_e \chi_M(R) \chi_i(R) \qquad \ldots(22)$$

where N_i = the number of frequencies of each species,

N_G = the number of element in the group,

n_e = the number of elements in each class,

$\chi_i(R)$ = the character of the vibration species.

The eq. (22) is used to determine the vibrations allowed in the infrared. Ferraro and Ziomek [84] described for the case of T_d. In the case of Raman spectrum, the character of the polarizability α, $\chi_\alpha(R)$, is used where

$$\chi_\alpha(R) = 2 \pm 2\cos\psi + 2\cos2\psi \qquad \ldots(23)$$

The values of $\chi_\alpha(R)$ appear in character table for each symmetry. The reduction formula is used as :

$$N_i = 1/N_G \, \Sigma n_e \chi_\alpha(R) \, \chi_i(R) \qquad \ldots (24)$$

2.14 Information about Selected Hydrates

2.14.1 $ZnHPO_4.H_2O$ and $Co(H_2PO_4)_2.2H_2O$

The acid inorganic salts, such as hydrogen phosphates, arsenates, sulphates, selenates, etc. are known to possess optical, electrical and magnetic properties of practical importance, which are determined by the presence of very strong hydrogen bonds in their crystal lattices. Among the acid phosphates the well-known compounds of the $MH_2PO_4.nH_2O$ series (M = Co, Ni, Zn) have been subject of numerous investigations because of interesting ferro- and antiferroelectric phase transitions, which occur at different temperatures.

Open framework materials are of significant interest due to a number of potential applications as heterogeneous selective catalysts, ion exchangers and molecular sieves. Recently, porous materials for gas adsorption are explored intensively [85–87]. In addition to its application in important metal products, a-hopeite is the crystalline reaction product of biomedical zinc phosphate cement, which is used to attach prefabricated crowns and inlays to teeth, to line cavities for the protection of dental pulp against chemical attack and thermal stresses, and even to fill cavities. Crystals of a-hopeite grow on the outermost surface of the cement, in direct contact to human dentine and enamel [88–92].

2.14.2 Dilithium Zinc Hydrogenphosphate Monohydrate $(Li_2Zn(HPO_4)_2.H_2O)$

Microporous materials are of great interest because of their widespread applications in catalysis, ion-exchange, adsorption and host-guest assemblies. The structure of lithium zinc hydrogenphosphate monohydrate consists of lithium, zinc and phosphorus atoms tetrahedrally coordinated to oxygen atoms. The three-dimensional framework structure can be described as belonging to the family of stuffed cristobalite structure with zinc and phosphorus atoms as tetrahedral framework atoms [93]. The extra-framework comprises of lithium and water molecule, which are

located in the cavity of the system [94]. Open-framework materials of aluminosilicates (zeolites) and aluminophosphates with varying dimensions are of great interest for their chemical and physical properties and plethora of other applications [95-97]. The most established non-zeolitic solids are the phosphate based open-framework materials, which display considerable structural diversity [98]. Of these, the metal phosphates, especially those of zinc, are interesting as they form structures similar to zeolites [99-100]. The water molecules in $Li_2Zn(HPO_4)_2.H_2O$ can be removed and rehydrated without destruction the structure under the temperature of lower than 200 °C, which is similar to the case of zeolites.

2.14.3 $M^IM^{II}PO_4.nH_2O$ (M^I = Li, M^{II} = Fe, Co, Ni, Mn)

Metal phosphate hydrates of type $M^IM^{II}PO_4.nH_2O$ (M^I = alkali, M^{II} = transition metal) form a wide families of compounds showing interesting properties which give rise to their potential uses as catalysts for selective oxidation reaction, being particularly effective for oxidative dehydrogenation [101], and the positive electrodes for lithium batteries, $M^IM^{II}PO_4$ [102].

Since the pioneering work of Padhi et al.[103], mixed cations orthophosphates $LiMPO_4$ (M = Fe, Co, Ni, Mn) isostructural to olivine are intensively studied as lithium insertion compounds for Li batteries. The generation of an appropriately high voltage is due to the presence of the polyanion $(PO_4)^{3-}$ with strong P-O covalency, which stabilizes the antibonding Fe^{2+}/Fe^{3+} state through and Fe-O-P inductive effect. The inductive effect may be described as the action of one group to effect the electrostatically electron distribution in other group. Thus, a change in distribution of the electrons modifies the force constant of the chemical bonds. Hence, it is interesting to investigate the structure, properties and electrochemical insertion reaction of hydrate form of $LiMPO_4$.

Group theoretical treatment of the internal modes of the phosphate ions in dittmarite compounds (the same as Table 2.8) yields [104] :

$$\Gamma_{\nu_1} = A_1 + B_2$$

$$\Gamma_{\nu_2} = A_1 + B_1 + A_2 + B_2$$

$$\Gamma_{\nu_3, \nu_4} = 2A_1 + B_1 + A_2 + 2B_2$$

Where the species A_1, B_1 and B_2 are both IR and Raman allowed, but A_2 is only Raman allowed. Thus two infrared active bands ($A_1 + B_2$) corresponding to the ν_1 mode and five infrared active bands ($2A_1 + B_1 + 2B_2$) for the ν_3 modes are expected to appear in the region of the P-O stretches. For the bending vibrations, the factor group analysis predicts three IR active bands ($A_1 + B_1 + B_2$) for ν_2 and five IR active bands ($2A_1 + B_1 + 2B_2$) for the ν_4 mode. In Raman spectra, two bands ($A_1 + B_2$) for ν_1 mode, four bands ($A_1 + A_2 + B_1 + B_2$) for ν_2 and six bands ($2A_1 + A_2 + B_1 + 2B_2$) for the ν_3 and ν_4, respectively, should be expected. The infrared spectra of dittmarite compounds were studied by Šoptrajanov and co-worker [106-110]. Despite the fact that some these contributions are rather old, the existence of very low HOH bending frequencies has been indicated [108].

Table 2.6 T_d – C_s – D_{2h}^{16} correlation table of phosphate ions (PO_4^{3-}) in LiFePO$_4$.3H$_2$O, LiCoPO$_4$.3H$_2$O LiNiPO$_4$.H$_2$O and LiMnPO$_4$.H$_2$O

Mode	Molecular Point Group	Site Group	Factor Group
	T_d	C_s	D_{2h}^{16}
ν_1	$A_1(1)$		$A_g(6)$
			$B_{1g}(6)$
ν_2	$E(2)$	$A'(6)$	$B_{2g}(3)$
			$B_{3g}(3)$
ν_3	$F_2(3)$	$A''(3)$	$A_u(3)$
			$B_{1u}(3)$
ν_4	$F_2(3)$		$B_{2u}(6)$
			$B_{3u}(6)$

Table 2.7 The C_{2v}-C_1-C_{2v}^7 correlation table for the three internal water modes and

the water librational modes

Water molecule internal vibrations

Mode	Molecular point group	Site group	Factor group
	C_{2v}	C_1	C_{2v}^7

ν_1, ν_2 — A_1

ν_3 — A_2

$A(3)$

$A_1(3)$, $A_2(3)$, $B_1(3)$, $B_2(3)$

Water molecule librations

Mode	Molecular point group	Site group	Factor group
	C_{2v}	C_1	C_{2v}^7

ρ_t — A_1

ρ_w — B_1

ρ_r — B_2

$A(3)$

$A_1(3)$, $A_2(3)$, $B_1(3)$, $B_2(3)$

Table 2.8 The C_{2v}-C_s-C_{2v}^7 correlation table for the three internal water modes and

the water librational modes(zy plane preserved)

Water molecule internal vibrations (zy plane preserved)

Mode	Molecular point group	Site group	Factor group
	C_{2v}	C_s	C_{2v}^7
ν_1, ν_2	A_1		$A_1(3)$
		$A'(3)$	A_2
ν_3	B_2	A''	B_1
			$B_2(3)$

Water molecule librations

Mode	Molecular point group	Site group	Factor group
	C_{2v}	C_s	C_{2v}^7
ρ_t	A_1		$A_1(1)$
ρ_w	B_1	$A'(1)$	$A_2(2)$
ρ_r	B_2	$A''(2)$	$B_1(2)$
			$B_2(1)$

Table 2.9 The C_{2v}-C_s-C_{2v}^7 correlation table for the three internal water modes and the

water librational modes(xz plane preserved)

Water molecule internal vibrations (xz plane preserved)

Mode	Molecular point group	Site group	Factor group
	C_{2v}	C_s	C_{2v}^7

Water molecule librations

Mode	Molecular point group	Site group	Factor group
	C_{2v}	C_s	C_{2v}^7